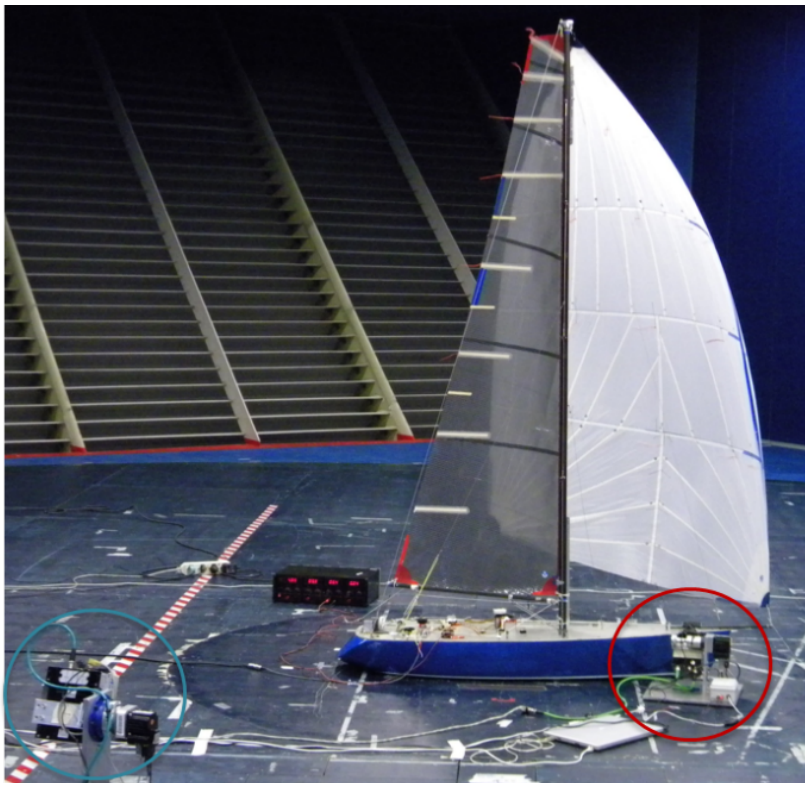

Figure 19 – The Flying Shape Detection (TOF) System and its position for wind tunnel tests: one system per sail

The device performs measurements in terms of spatial coordinates of thousands of points belonging to the sail surface without impairing its shape since no contact occurs between object and sensor. These data, coming singularly from two different laser scanners, one for main sail and the other for jib (or gennaker), as in Figure 19, are then processed together to reconstruct the 3D sail surfaces (Figure 20), which can be sectioned coincident with the pressure strip heights allowing comparison of the pressure distribution for a given sail shape (Figure 30). The scanning procedure takes only few seconds and gives the steady state configuration of the sail plan.

The test procedure was set to characterize the aerodynamic behavior of a sail plan at fixed heel and apparent wind angle. The sail trimmer acts on the control system to obtain the desired sails regulation. In order to properly trim he can use some cameras placed onboard the model to give a view similar to the real life (Figure 21) and the aerodynamic forces signal available in real time. The tests were performed at a velocity of about $U = 4\,m/s$, a compromise between higher signals and lower forces acceptable for the sail control system: the wind tunnel speed is mostly limited by the strength of the model mast and rigging and the power of the sheet winches.

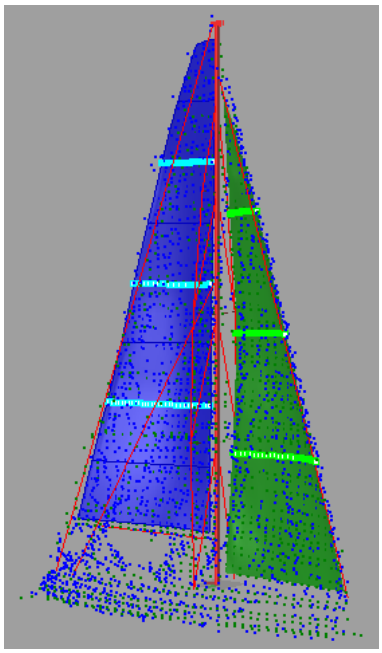

Figure 20 - Example of a point cloud acquired for mainsail (blue) and jib (green): 3D reconstruction sail shapes, highlighted sections in correspondence of the pressure strips

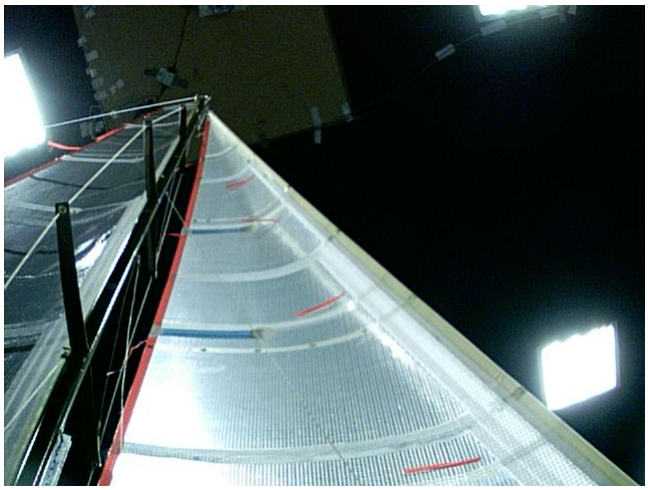

Figure 21 - Onboard camera view on jib during testing

Upwind sails tests and results

The usual way to analyze data of this type of measurements is comparison of non-dimensional coefficients (Fossati et al. 2006, Fossati et al. 2008), allowing to compare the efficiency of sails of different total area at different conditions of dynamic pressure. The first useful parameter to be analyzed is the variation of driving force coefficient Cx versus heeling force coefficient C_y. Figure 22 shows Cx vs Cy curves for the 6 Apparent Wind Angles (AWA) tested in this campaign. It can be seen that there are some settings at the highest values of heeling force coefficients where the driving force is lower than the maximum value (e.g. below the maximum efficiency curve, isolated points in Figure 22). These non-optimum values were due to an over-sheeting of the sails, such that the mainsail generally had a tight leech and the airflow separated in the head of the sail, (Abbott et al. 1959). After having maximized the driving force, the sails were adjusted to reduce the heeling force while observing the reduction of the driving force. The reduction in heeling force was achieved by initially easing the main sheet, to twist the mainsail and minimize flow separation, then adjusting the traveller to reduce the angle of attack of the wind on the main. Envelope curves

have been drawn through the test points with the greatest driving force at a given heeling force (e.g. depower curves, Figure 22).

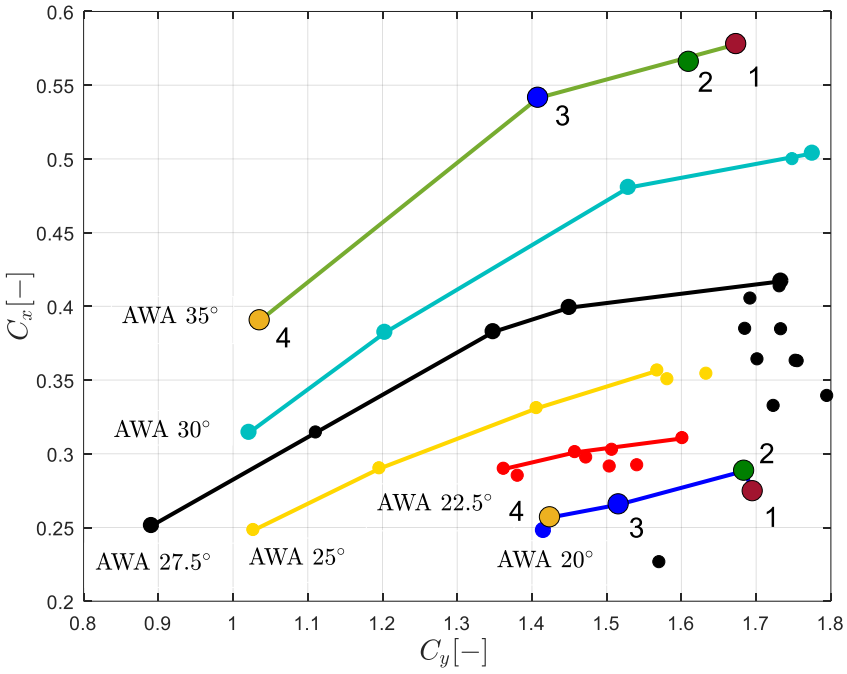

Figure 22 - Driving force coefficient C_x versus lateral force coefficient C_y

Two other interesting parameters used to characterize a sail plan are the positions of the center of effort in terms height (Ceh) and in terms of the longitudinal position (Cea). They are calculated as:

$$Ceh = \frac{M_x}{F_y h_{mast}} \tag{2}$$

$$Cea = \frac{M_z}{F_y \mathrm{LWL}} \tag{3}$$

where M_x is the roll moment, F_y the heeling force, h_{mast} the height of the mast, M_z the yaw moment and LWL the length of the water line. Both Ceh and Cea reported in Figure 23 are normalize over a reference length.

As it can be seen, the center of effort height tends to decrease as the heeling force coefficients decrease. This is explained by the way in which the sails are de-powered to reduce C_y: increasing the twist reduces the loading in the head of the sails and then depowering the mainsail leaving the same genoa trim, which has a lower center of effort, tends to reduce it. On the other hand, Cea moves forward as C_y reduces: this is again explained by the way the sails are de-powered.

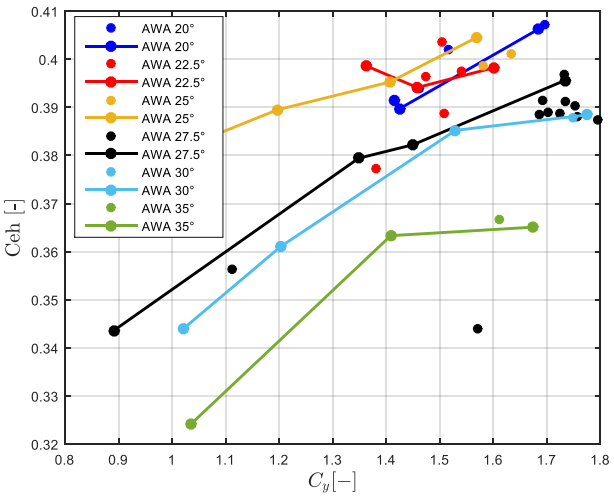

(a) Centre of effort height vs heeling force coefficient

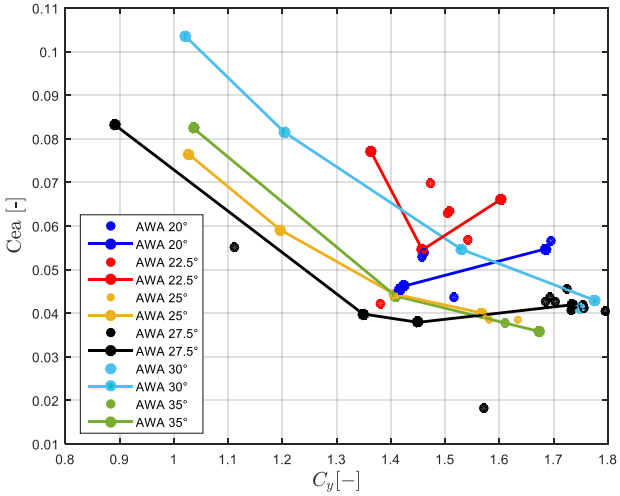

(b) Centre of effort longitudinal position vs heeling force coefficient

Figure 23 - Position of the center of effort

For each point plotted in Figure 22 and in Figure 23 pressure distributions over the two sails were measured:

For a preliminary qualitative analysis, the schematic pressure drawings published in Viola et al. 2011a (Figure 24) can be used as reference: the obtained distributions, especially on the middle sections (see Figure 25) of main and jib, present evident agreement with the expected trends. Comparing Figure 24 and Figure 25 it can be noticed that the main trend is visible, whereas the negative pressure in Figure 25 are bit higher: this can be explained considering the reasonable differences in terms of sail shape and surface roughness.

Both sails present a suction region, on the leeward side, where the flow is accelerated and the pressure drops, and a region of positive pressure on the windward side where the flow is slowed down. At the leading edge of both sails, the flow detaches from the surface and reattaches further downstream creating the so-called separation bubble, which is a region of recirculating flow. At the trailing edge, depending on the sail trim and the angle of attack with the incoming air, the flow might separate again leading to turbulent phenomena and vortex shedding.

In general, the aerodynamic loads on the headsail are greater and oriented more towards the forward direction compared to the main sail; this characteristic is due to the different shape of the two sails and their interaction with each other. The mainsail positively affects the jib by increasing its effective angle of attack (up-wash effect) and accelerating the flow on the leeward side thanks to the suction region created; to the contrary, the headsail acts oppositely on the main (down-wash effect) which therefore is subjected to lower aerodynamic loads.

Some studies expanded this subject, identifying different regions in which attached flow, separation bubbles, reattaching phenomena and detached flow alternate with each other (Wilkinson 1989, Viola et al. 2011a, Viola et al. 2011b, Crompton et al. 2000). It was interesting as in the case of the mainsail, to see that the mast plays an important role in the creation of the separation bubble while for the headsail, even though it does not have any large bluff body in front, the leading edge often presents a separation bubble and the high curvature of the sail might lead to flow separation at the trailing edge.

With reference to Figure 26 (Viola et al. 2011b), the separation bubble on the leeward side occurs when the angle of attack is higher than the ideal one, that is when the sail leading edge is not exactly aligned with the streamlines of the incoming flow. In case of soft sails, a slightly over-tightened trim of this kind is desirable in order to prevent the sails from flapping; therefore, separation bubbles are often present.

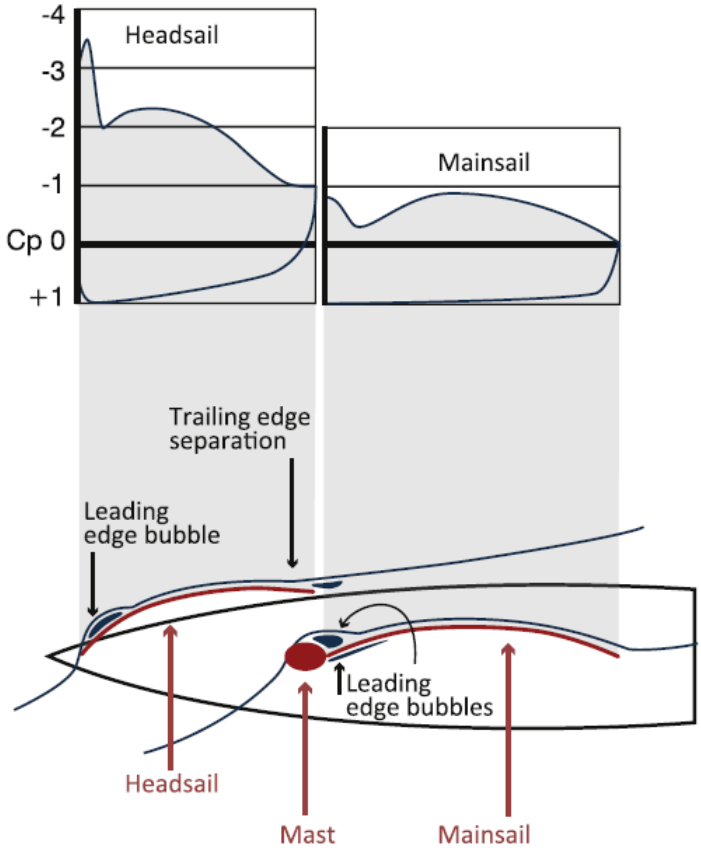

Figure 24 - Expected pressure distributions on the mid sections of the two sails (Viola et al. 2011a)

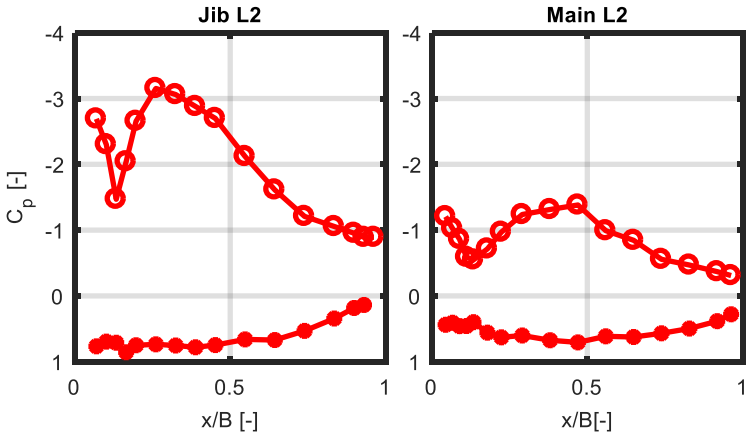

Figure 25 - Pressure distribution measured at $AWA = 20°$, level L2, maximum drive force condition

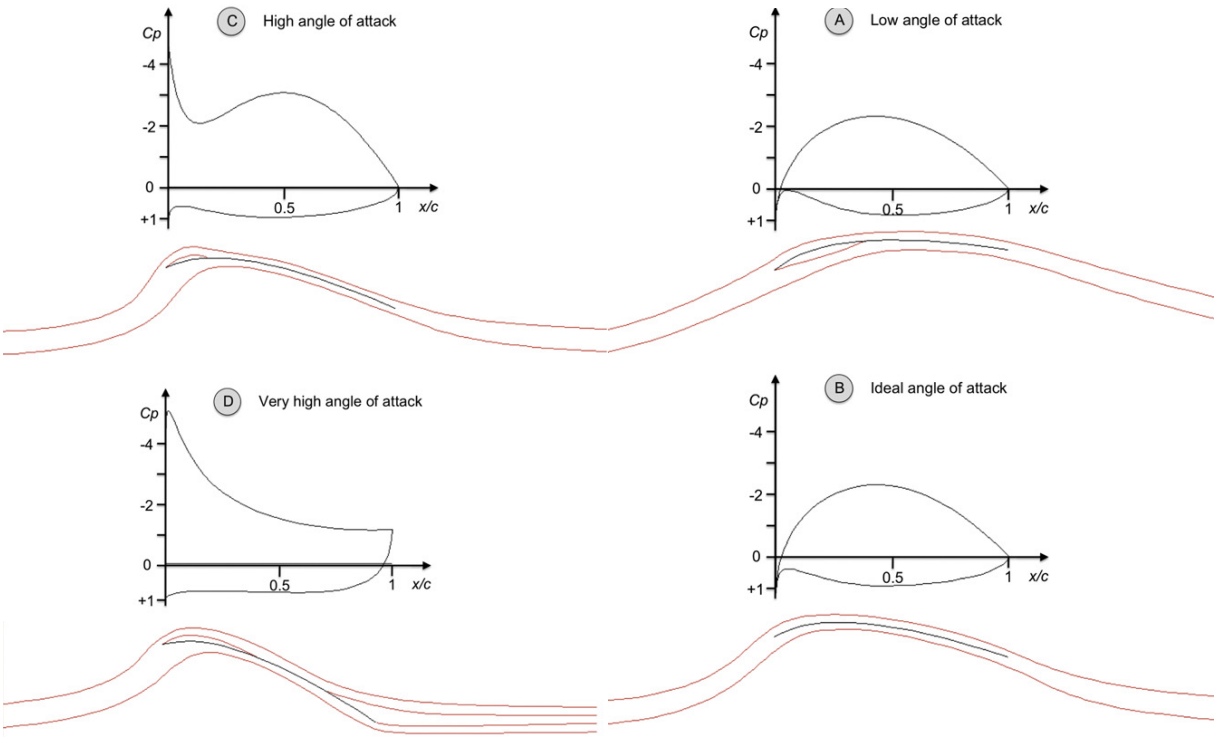

Figure 26 - Expected C_p distributions along the headsail sections at varying angles of attack (Viola et al. 2011b)

Next, for a more thorough analysis of the local pressure characteristics, the sail sections will be presented by means of two-dimensional scaled graphs. First, the differences of load distributions on sails due to the depowering procedures will be discussed; second, the influence of the variation of wind angle will be evaluated.

As depicted in Figure 22, the points laying on the de-powering curve at maximum and minimum apparent wind angle $AWA = 35°$ and $AWA = 20°$were chosen for a more thorough investigation in terms of pressure distributions and corresponding flying shapes. More specifically, as can be noticed in Figure 13 and in Figure 17, three stations at different height, both on mainsail and jib, port/starboard sides, were chosen for application of the pressure strips on (Figure 13 and Figure 20). L1, L2 and L3 stand for the three levels at 25%, 50% and 75% of the sail heights respectively, so the corresponding pressures at points 1-4 are reported in Figure 27 and in Figure 28

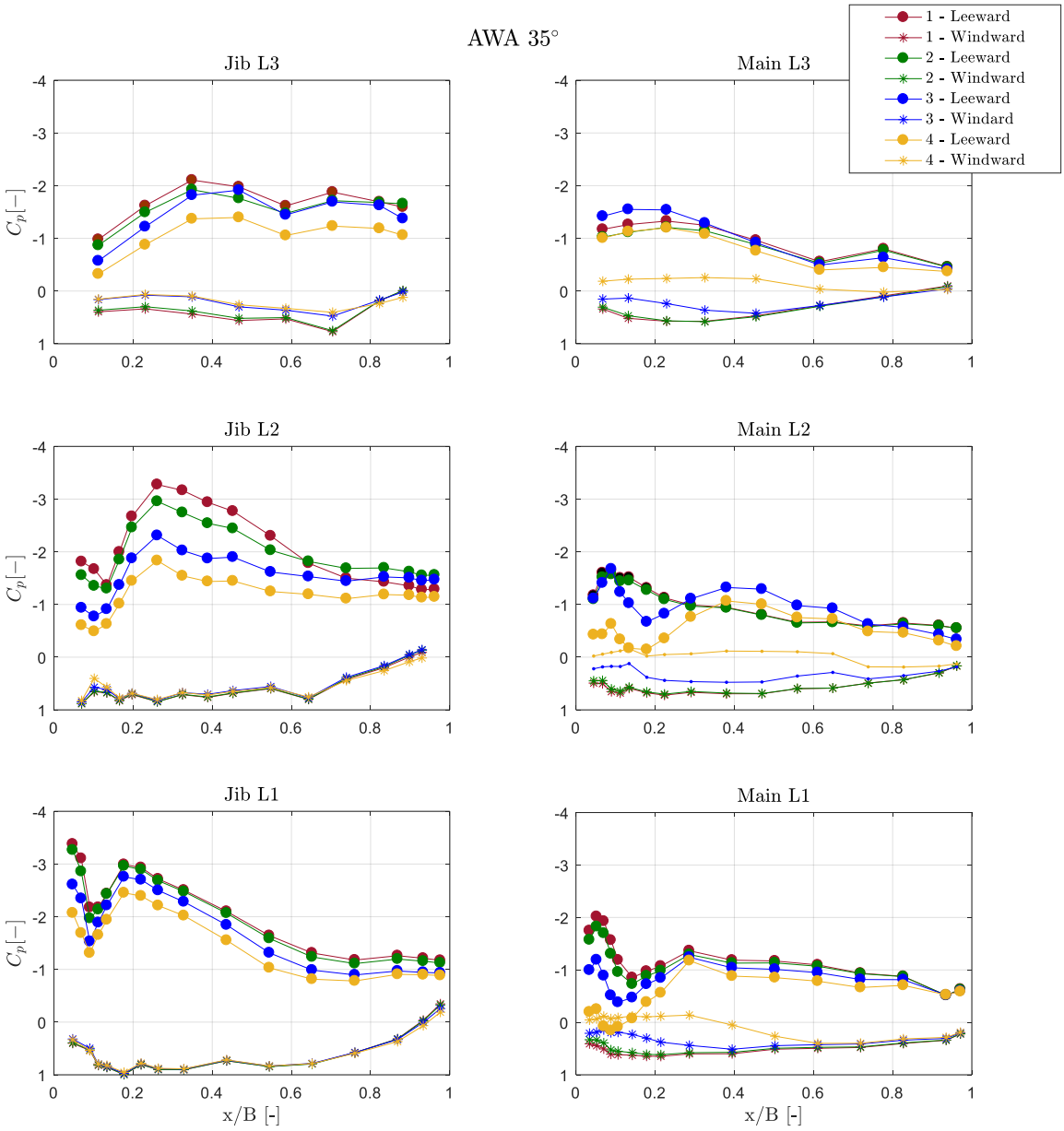

Figure 27 - Pressure distributions on the three stations along the span of the sail plan: points on the maximum power curve for an apparent wind angle $AWA = 35°$

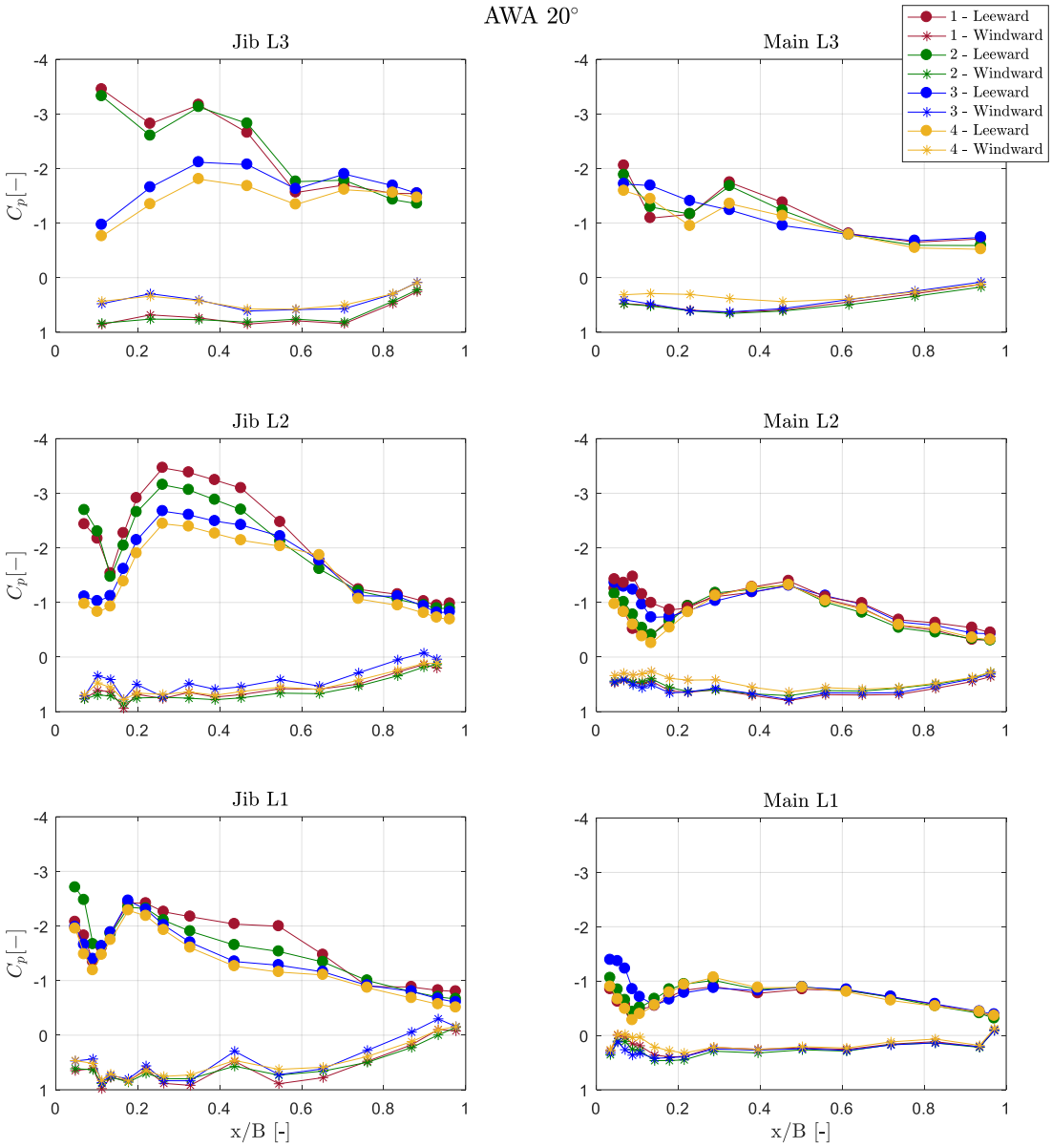

Figure 28 - Pressure distributions on the three stations along the span of the sail plan: points on the maximum power curve for an apparent wind angle $AWA = 20°$

From a first look, all the trends obtained present characteristics in accordance to the reference studies present in literature as observed before: it is possible to recognize the different flow features described, such as leading edge separation bubble, curvature-related suction peaks and trailing edge pressures, are all clearly visible both on main and jib experimental distributions. This is particularly true for the middle sections where the flow is not disturbed by tip effects. Starting from the main sections, as expected, the mast has great influence on the pressure distribution and interestingly, the effect varies along the sail height and with trim. For both of the angles considered an increase of the negative pressure coefficients can easily be seen in the leeward side near the leading edge, where the mast is placed: as discussed before this is related to a large separation bubble that extends up to 10% of the chord. The highest negative values in this region were obtained for the powerful configurations while when easing the main the flow is less accelerated and consequently

the negative values became lower. In these cases, the greater sail curvature leads to higher (more negative) pressure gradients that allow reaching similar values at the middle of chord; from that location, the downstream distribution remains almost identical within the same depower curve. Furthermore, moving along the airfoil chord, up to the trailing edge, another greatly negative pressure coefficient region is experienced. For $AWA = 20°$ all the considered points show a second separation region, while for $AWA = 35°$ only the points at lower driving force coefficient C_x (i.e. 3-4in Figure 22) have this region. For points with greater efficiency (i.e. 1-2 of Figure 22) this bubble seems not to be occurring: therefore, after the separation due to the mast, a monotonic trend up to the trailing edge is evident, indicating a gradual and efficient reattachment of the flux on the leeward side of the sail. These differences related to the angle of attack will be discussed more in detail in the following.

At the trailing edge, the pressure tends to level off at constant values indicating partial flow detachments that prevent the pressure to fully recover.

Regarding the headsail, it is worth recalling that its shape was not changed during the depowering procedure; therefore, the pressure distribution differences between the various trims must be attributed to the changes of the mainsail's influence only. In particular, a more powerful suction on the main's leeward side, corresponds to a stronger up-wash effect which, in turn, results in greater induced angles of incidence.

With reference to the 20° case (Figure 28), it is evident how the changing angle influences the jib's leeward pressure distribution, especially at the leading edge. More specifically, when the up-wash effect is very strong, i.e. the angle of incidence very high (trims 1 and 2), the pressure at the leading edge reaches considerably low values and the separation bubble enlarges. As the main is eased, the up-wash induced angle of attack of the jib decreases and the leading edge bubble gets smaller.

Also for the 35° case a similar behavior was observed (Figure 31 particularly in the middle section (L2).

The different lifting attitude of the jib revealed by the measured pressure distributions can be considered the main source of the driving force reduction along the de-power curve.

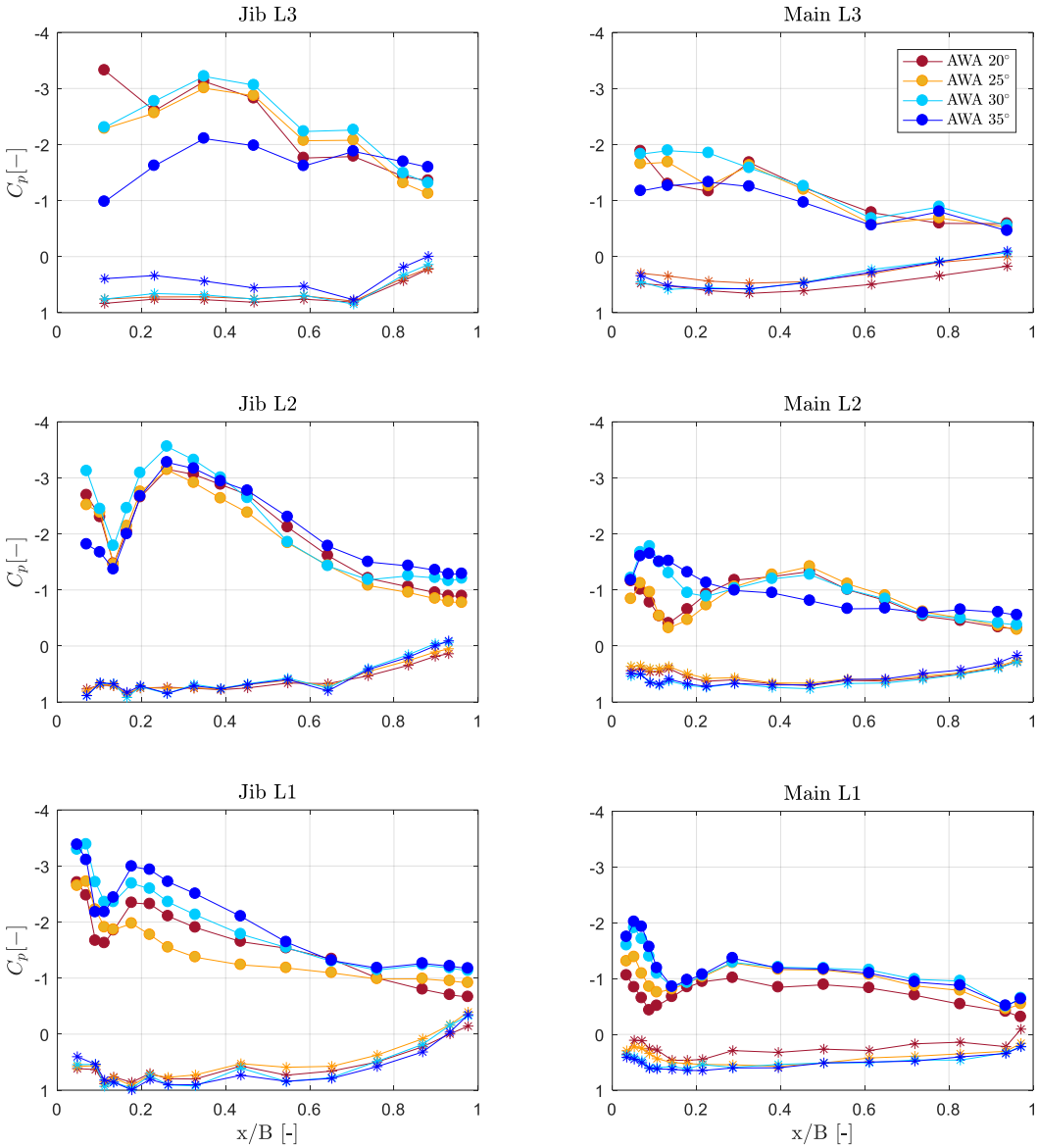

Figure 29 - Comparison of the pressure distribution of different apparent wind angles AWA (20°, 25°, 30° and 35°) both considered at the maximum driving force coefficients

In order to consider the AWA effect on the pressure distributions, in Figure 29, a comparative plot of 4 different AWA (20°, 25°, 30° and 35°), all from maximum driving force coefficient configurations (see Figure 22), is reported. Considering again the section L2 both for jib and for main, without loss of generality for the other sectional airfoils, the following explanations can be drawn: the pressure distributions of the jib have basically similar trends and values, indicating there exists an optimum shape that maximizes the aerodynamic efficiency of the sail. Nevertheless, at increasing wind angles, this same regulation results in growing angles of attack that lead to strong leading edge negative peaks.

The main differences, especially in terms of values can be noticed on the mainsail's distributions. The different orientation of the mast, which has an elliptical section, together with the different sail curvatures for the angles considered, generates suction peaks of

different intensity especially at the leading edge. At 30° and 35° the mast remarkably accelerates the flow, resulting in a separation bubble with high mean velocity, as the AWA decreases, the angle of attack of the mast reduces weakening the flow acceleration and, consequently, the intensity of the depression.

This difference results in different driving forces and in different center of effort positions.

In order to better understand how the pressure distributions are related to overall aerodynamic force, pressure and sails shape are considered at once. Figure 30 shows the pressure distribution for $AWA = 20°$ in the maximum driving force condition corresponding to section L2: the pressure are directly plotted on the measured section with blue arrows corresponding to positive pressure coefficients (windward), whereas red ones to negative (leeward). From this representation, it is clear that the driving force, computed as the integral of the pressure distribution on the corresponding section, is mainly contributed by the jib.

Comparing Figure 27 and Figure 28 is also interesting to notice that a less efficient sail plan (e.g. pt.4 of $AWA = 35°$, Figure 27) is aerodynamically similar to a sail plan set to a smaller effective apparent wind angle ($AWA = 20°$ Figure 28), which is something that is also known and commonly experienced in sailing. As a matter of fact, great similitude can be found in the results reported in Figure 27 and Figure 28, with the extensively investigated aerodynamics of airfoils with external airfoil flaps (Abbott et al. 1959).

The same considerations can be drawn analyzing pressure distributions along with the sail shapes detected by TOF system. More specifically, in Figure 31 a comparative visualization of the pressure distributions on the effective flying shape, at the corresponding section (L2), is reported for the apparent wind angle $AWA = 35°$ and for maximum and minimum efficiency (i.e. pt.1 and 4 of Figure 22).

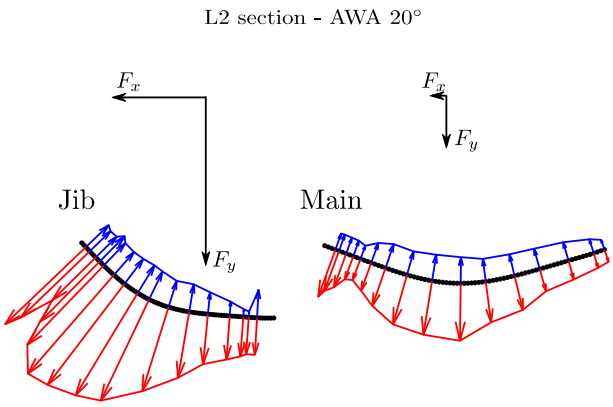

Figure 30 - Visual pressure distribution on the sail plan based on measurements at section L2, $AWA = 20°$

The pressure distributions are the same as reported in Figure 27. It is evident how basically the same jib's shape of the section, which was not modified along the de-power curve of Figure 22, results in different pressure trends due to the different efficiency of the mainsail, whose suction effect on the jib is greatly lower in a de-powered setting. Also the different overall lateral forces F_y depicted in Figure 30, computed from integrating the pressures over the L2 section, confirm the integral measurements reported in Figure 22. Furthermore, in Figure 32, the comparison of different AWA results (20° and 35°, also reported in Figure 28), both in a maximum power configuration, for L2 section, are shown in terms of pressure/shape visualizations. It is easy to notice that the fairly similar pressure distribution on the jib due to the maximum power based trimming, is associated with different shape, leading to different driving forces on the jib and comparable lateral forces on the mainsail

(i.e. Figure 22, for approximately the same C_y, $AWA = 20°$ shows a lower driving force coefficient C_x with respect to $AWA = 35°$). Also Figure 33, in which apparent wind directions are highlighted, supports the consideration reported above: more specifically, the less efficient sail plan at $AWA = 35°$ shows similarities with lower AWA configurations in terms of mainsail pressure distribution. In fact, a reattachment of the flow right behind the mast combined with the co-alignment of the flow with the luff of the mainsail is quite evident.

It is worth mentioning that these tests represent, according to author's knowledge, one of the first wind tunnel set of measurements of the pressure distributions on flexible sails, instead of rigid, which is a testing condition closer to the real navigation (i.e. full scale), whose measurements (forces, pressures and flying shapes) on Sailing Yacht Laboratory, will take advantage of the present research.

Furthermore, the rationale behind the way the sails were trimmed, corresponds to a procedure which is consistent to the real sailing navigation. However, a systematic investigation on the aerodynamics of sail plans, relying on this experimental setup, could be based on different depowering approaches, aiming at assessing the effect of single trim parameters (involving the jib also) on the local and integral efficiency of the sails.

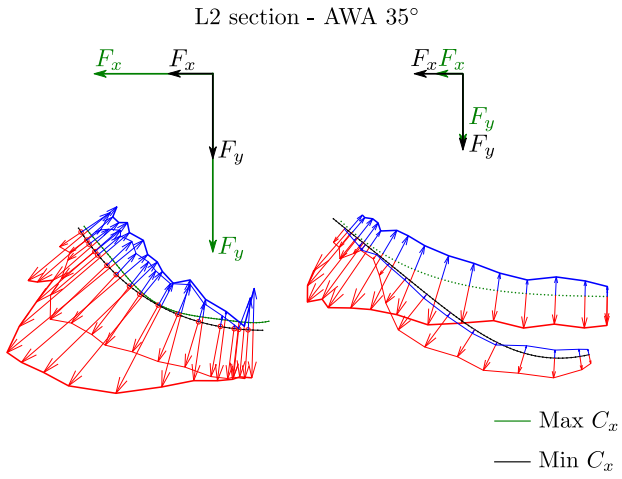

Figure 31 - Pressure distributions for L2 section for $AWA = 35°$, maximum and minimum power configurations

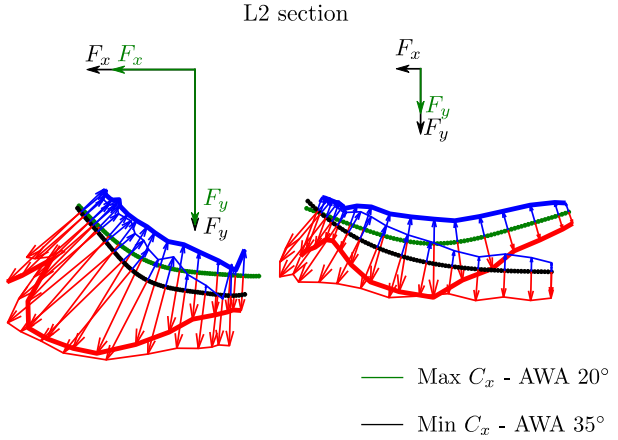

Figure 32 - Pressure distributions for L2 section, maximum power configuration, $AWA = 20°$ and $AWA = 35°$

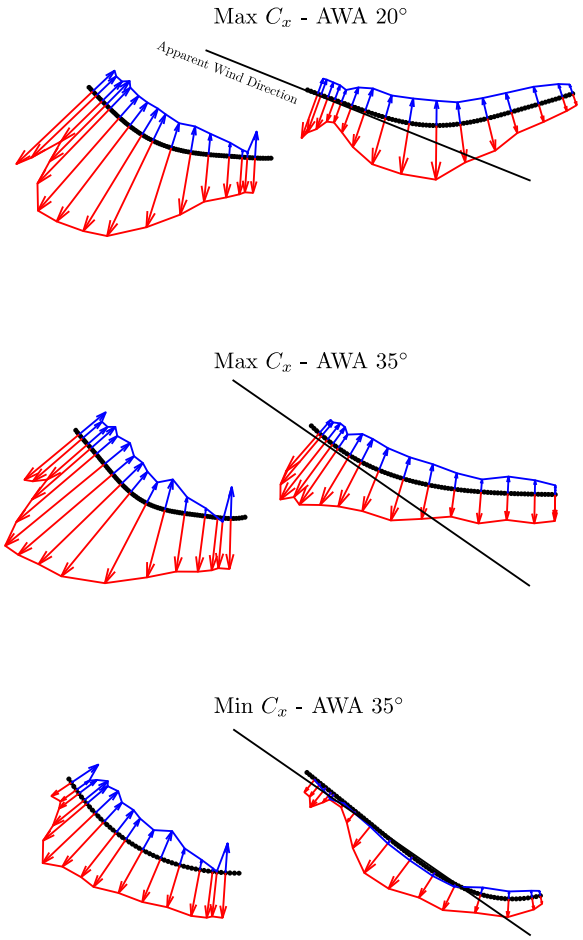

Figure 33 - Pressure distributions for various AWA and power configurations

FULL SCALE PRESSURE SYSTEM LAYOUT

On the Sailing Yacht Lab, the pressure distribution on the sails is carried out by means of specifically designed pressure pads which have been designed and produced aiming to provide the differential measurement between the sail leeward and windward side. The above reported metrological characterization of the strips and the wind tunnel tests were mainly to assess the capabilities of the measuring system, in advance with respect to the final full scale implementation with pads. However, during the wind tunnel tests some tests on pads themselves were conducted just to verify they functioned as expected, Figure 34. With reference to the Sailing Yacht Laboratory sail inventory, Figure 35 and Figure 36 show the proposed sail pressure measurement system, the sections considered and a relevant number of pressure taps for the complete sail plan. The full scale pressure system is being finalized at the time of writing this paper.

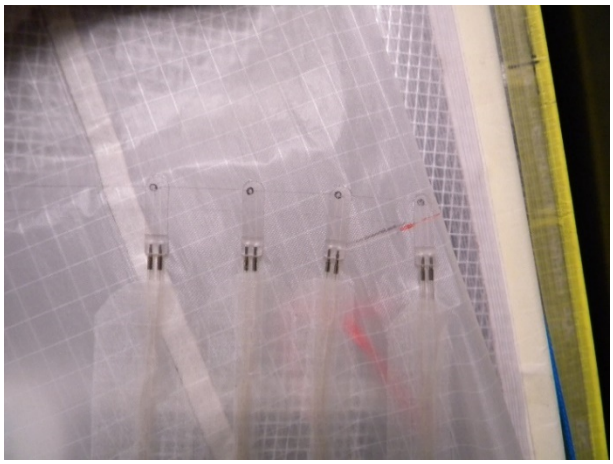

Figure 34 - Example of the full scale pads on gennaker sail for wind tunnel model

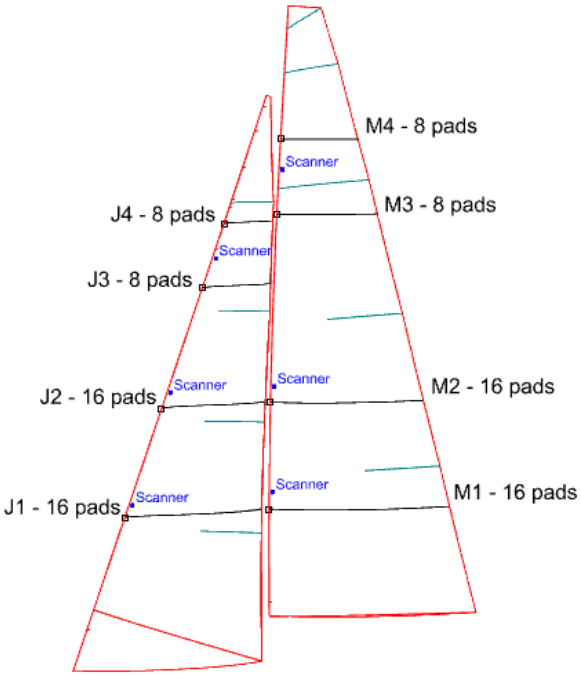

Figure 35 - Full scale mainsail and jib pressure taps layout

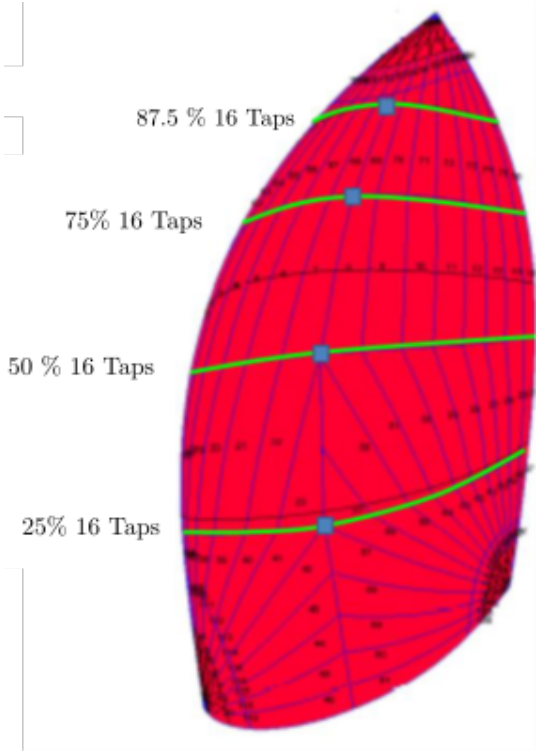

Figure 36 - Full scale gennaker pressure taps layout

CONCLUSIONS

A joint project developed among Politecnico di Milano, CSEM and North Sails, aiming at developing a new sail pressure measurement system is presented in the paper. The system was designed for the specific application of full scale measurements on Politecnico di Milano Sailing Yacht Laboratory.

The capabilities of this system were evaluated through a metrological validation of the system alone (static and dynamic tests) and through wind tunnel tests in the upwind configuration. The pressure system was integrated in the existing set up, in particular together with flying shape detection based on time of flight technology.

Wind tunnel tests allowed checking the reliability of the new system and investigating thoroughly upwind soft sail aerodynamics, with the possibility of carrying out sail trim as in real navigation. During the wind tunnel test session, each side of the sail pressure distribution was measured with reference to a common static pressure, by means of pressure strips, whereas for full scale implementation, pressure pads for differential measurements were developed.

Wind tunnel results give a promising preview of the potential of the system described in explaining the dependency of sail plan aerodynamics on sail trim, relying on the combined measurements of forces, pressures and flying shapes.

Furthermore, these measurements will represent a great reference database for validation of CFD codes and can be used to complete the interpretation of full scale results.

Further developments in the visualization techniques (particle image velocimetry) are expected to be combined with this methodology in the near future.

ACKNOWLEDGEMENTS

The authors want to thank the master student Riccardo Romagnoni for his help in performing the calibration tests.

REFERENCES

Abbott H., Doenhoff E., Theory of Wing Sections: Including a Summary of Airfoil Data, Dover Publications, Inc. New York, 1959.

Crompton, M. J., Barrett, R. V, “Investigation of the separation bubble formed behind the sharp leading edge of a flat plate at incidence”, Proc. Inst. Mech. Eng. Part G J. Aerosp. Eng., vol. 214, pp. 157–176, 2000.

Deparday, J., Bot, P., Hauville, F., Motta, D., Le Pelley, D.J., Flay, R.G.J., Dynamic measurements of pressures, sail shape and forces on a full-scale spinnaker, in 23rd HISWA Symposium on Yacht Design and Yacht Construction, Amsterdam, 2014

Fossati, F., Muggiasca, S., Maria, I., Zasso, A. Wind tunnel techniques for investigation and optimization of sailing yachts aerodynamics (2006) 2nd High Performance Yacht Design Conference 2006, pp. 105-113.

Fossati, F., Muggiasca, S., Martina, F. Experimental database of sails performance and flying shapes in upwind conditions, in INNOVSAIL International Conference on Innovation in High Performance Sailing Yachts, Lorient, RINA, pp. 99-114, 2008.

Fossati, F., Muggiasca, S. Experimental investigation of sail aerodynamic behavior in dynamic conditions (2013) Transactions - Society of Naval Architects and Marine Engineers, 120, pp. 327-367.

Fossati F., Bayati I., Orlandini F., Muggiasca S, Vandone A., Mainetti G, Sala R., Bertorello, Begovic E: “A Novel Full Scale Laboratory For Yacht Engineering Research”, Ocean Engineering 104 (2015) 219-237.

Fossati F., Mainetti G., Sala R., Schito P., Vandone A., “Offwind Sail Flying Shapes Detection, 5th, High performance Yacht Design Conference, Auckland, 2015.

Le Pelley, D., Morris, D., Richards, P., "Aerodynamic force deduction on yacht sails using pressure and shape measurements in real time", in 4th High Performance Yacht Design Conference, Auckland, pp. 28–37, 2012.

Lozej, M., Golob, D., Bokal, D., "Pressure distribution on sail surfaces in real sailing conditions", in 4th High Performance Yacht Design Conference, Auckland, pp. 242–251, 201, 2012.

Motta, D., Flay, R.G.J., Richards, P.J., Le Pelley, D.J., Deparday, J., Bot, P., "Experimental investigation of asymmetric spinnaker aerodynamics using pressure and sail shape measurements", Ocean Engineering, 90, pp. 104-118, 2014.

Motta, D., Flay, R.G.J., Richards, P., Le Pelley, D.J., Bot, P., Deparday, J., An investigation of the dynamic behavior of asymmetric spinnakers at full-scale, in 5th High Performance Yacht Design, Auckland, 2015

Pot, P., Viola, I.M., Flay, R.G.J., Brett, J.S., Wind-tunnel pressure measurements on model-scale rigid downwind sails, Ocean Engineering, 90, pp. 84-92, 2014

Tijedman, R., Berg., M. T. "Theoretical and experimental results for the dynamic response of pressure measuring systems", Technical Report NLR-TR F.238, 1965

Viola, I.M., Flay, R.G.J., "Sail pressures from full-scale, wind-tunnel and numerical investigations", Ocean Engineering, 38 (16), pp.1733–1743, 2011a.

Viola, I.M., Flay, R.G.J, “Sail aerodynamics: Understanding pressure distributions on upwind sails”, Exp. Therm. Fluid Sci., vol. 35, no. 8, pp. 1497–1504, 2011b.

Viola, I.M., Flay, R.G.J., "Sail aerodynamics: on-water pressure measurements on a downwind sail', Journal of Ship Research, 56(4), pp.197-206, 2012.

Wilkinson, S. “Static pressure distributions over 2D mast/sail geometries”, Mar. Technol., vol. 26, no. 4, pp. 333–337, 1989.